



ELSEVIER

Contents lists available at ScienceDirect

Biosensors and Bioelectronics

journal homepage: www.elsevier.com/locate/bios

Electrical detection of dengue virus (DENV) DNA oligomer using silicon nanowire biosensor with novel molecular gate control



M. Nuzaihan M.N.^{a,*}, U. Hashim^{a,b}, M.K. Md Arshad^{a,b}, S.R. Kasjoo^b, S.F.A. Rahman^c,
A.R. Ruslinda^a, M.F.M. Fathil^a, R. Adzhri^a, M.M. Shahimin^b

^a Institute of Nano Electronic Engineering, Universiti Malaysia Perlis (UniMAP), 01000 Kangar, Perlis, Malaysia

^b School of Microelectronic Engineering, Universiti Malaysia Perlis (UniMAP), 02600 Pauh, Perlis, Malaysia

^c Chemistry Department, Faculty of Science, Universiti Putra Malaysia, 43400 UPM Serdang, Selangor, Malaysia

ARTICLE INFO

Article history:

Received 26 February 2016

Received in revised form

11 April 2016

Accepted 12 April 2016

Available online 14 April 2016

Keywords:

Dengue fever (DF)

Deoxyribonucleic acid (DNA)

Silicon nanowire biosensor

Electrical detection

Molecular gate control

Nanolithography

ABSTRACT

In this paper, a silicon nanowire biosensor with novel molecular gate control has been demonstrated for Deoxyribonucleic acid (DNA) detection related to dengue virus (DENV). The silicon nanowire was fabricated using the top-down nanolithography approach, through nanostructuring of silicon-on-insulator (SOI) layers achieved by combination of the electron-beam lithography (EBL), plasma dry etching and size reduction processes. The surface of the fabricated silicon nanowire was functionalized by means of a three-step procedure involving surface modification, DNA immobilization and hybridization. This procedure acts as a molecular gate control to establish the electrical detection for 27-mers base targets DENV DNA oligomer. The electrical detection is based on the changes in current, resistance and conductance of the sensor due to accumulation of negative charges added by the immobilized probe DNA and hybridized target DNA. The sensitivity of the silicon nanowire biosensors attained was $45.0 \mu\text{A M}^{-1}$, which shows a wide-range detection capability of the sensor with respect to DNA. The limit of detection (LOD) achieved was approximately 2.0 fM. The demonstrated results show that the silicon nanowire has excellent properties for detection of DENV with outstanding repeatability and reproducibility performances.

© 2016 Elsevier B.V. All rights reserved.

1. Introduction

Today, the increasing outbreaks of dengue fever (DF) have become a major global problem. Approximately 3.6 billion people in 124 countries (55% of the world's population) are at risk for DF, with the expectation of more than 100 million cases yearly (Lee et al., 2015; Rathakrishnan and Sekaran, 2013; Teoh et al., 2015). This outbreak is seriously affected in the South East Asia and the Western Pacific (in the tropical and subtropical regions) (Darwish et al., 2015; De Paula and Fonseca, 2004; Gubler, 1998; Lee et al., 2015), which is a leading cause of hospitalization and death when compared with other diagnoses or diseases of humans (Cheah et al., 2014).

According to the data from Malaysia Ministry of Health (MOH), Malaysia is one of the worst affected countries, in which 59,365 cases of DF with 165 deaths have been reported from January to July 2015 in all states across the country. This is 33.4% higher compared with the same reporting period of 2014. Therefore,

* Corresponding author.

E-mail address: m.nuzaihan@unimap.edu.my (M. Nuzaihan M.N.).

Malaysia MOH has implemented various measures (e.g., dengue vector control, awareness campaign and early treatment) to reduce the incidence of dengue cases and save human lives (Cheah et al., 2014; Lee et al., 2015). In addition, the methods for diagnosing DF or detecting the dengue virus (DENV) at a very early stage are urgently needed to prevent the spreading of the outbreaks.

In recent years, biosensor technologies play an important role in the detection of the DENV not only because of their excellent potential to satisfy the high detection specificity and sensitivity (Abdul Rashid et al., 2016; Izuan et al., 2014; Oliveira et al., 2011; Silva et al., 2015; Wu et al., 2005), but also because they are rapid (Dias et al., 2013; Huang et al., 2013; Rai et al., 2012; Chen et al., 2009a, 2009b), portable and cost-effective method (Baeumner et al., 2002; Figueiredo et al., 2015; Oliveira et al., 2015; Rashid et al., 2015; Zhang et al., 2010). Biosensor is an analytical device that transfers a biological (molecular) reaction into an electrical signal via two main components, which are the sensing device (transducer or detector elements) and the sensing molecule (biological or biochemical components) (Li et al., 2014; Shalev et al., 2013). According to literature review, biosensors can be classified by types of transduction. The most common types of transduction

used in biosensors are electrical, electrochemical, piezoelectric, optical etc. (Monošik et al., 2012; Rashid et al., 2015; Teles et al., 2005).

Presently, with the advancement in the transduction of analytical signals in molecular into electrical signals, many efforts in the electrical biosensor have been made to develop and improve the sensitivity in the detection of the DENV DNA (Huang et al., 2013; Zhang et al., 2010). These electrical biosensors have been designed by using transducers with nanoscale structures, such as nanowires, nanotubes and nanoparticles, since the dimension is comparable to the feature sizes of chemical and biological species to be sensed (Fathil et al., 2015; Zhang and Ning, 2012). Among these transducers, the nanowires have demonstrated great sensitivity to the detection of biomolecular species, with limits of detection (LOD) can achieve down to femtomolar concentrations (Adzhri et al., 2016; Shalev et al., 2013). Silicon nanowires are fabricated either via bottom-up (Hahm and Lieber, 2004; Patolsky et al., 2006; Schmidt et al., 2010) or top-down approach (Agarwal et al., 2008; Chen et al., 2009a, 2009b; Kong et al., 2012; Md Nor et al., 2013; Noor and Krull, 2014; Ryu et al., 2010; Tian et al., 2011; Za'bah et al., 2012). Both approaches are able to produce silicon nanowires in the range of ~ 1 –100 nm with their own unique properties (electronic, mechanical and optical), a good biocompatibility, and a large surface to volume ratio. In addition, silicon nanowires have demonstrated an excellent electrical detection with good holes or electrons transfer in the detection due to the accumulation or depletion of charge inside nanowire, resulting in a greater effect of the conductance, resistance and faster response of detection when compared with other devices (Abdul Rashid et al., 2013; Gao et al., 2007; Kong et al., 2012; Patolsky et al., 2004; Yang and Zhang, 2014). Furthermore, our preliminary studies showed that the electrical detection based on silicon nanowire has a good potential not only as a pH sensor (Nuzaihan et al., 2015) but also in detecting Deoxyribonucleic acid (DNA) (Adam and Hashim, 2015, 2016).

To the best of our knowledge, the development of p-type silicon nanowire biosensor for the detection of DENV has been so far largely unexplored. Because of the potentials and important applications of the electrical biosensor to reduce and diagnose large populations suffering from the outbreaks of DF, for the first time, we report herein an electrical detection of DENV DNA oligomer using p-type silicon nanowire biosensor (device) with novel molecular gate control. Our p-type silicon nanowire worked, as a sensing element of the device is sandwiched between the source (S) and the drain (D) electrodes. The device is then functionalized with a bio-receptor, which is served as a “molecular gate” by the binding of a target DNA. The interaction of the target molecules with the bio-receptor has effectively been detected by monitoring electrical detection in response to the concentrations of DENV DNA with greatly enhanced of sensitivity and the detection limit as low as femtomolar concentrations. In addition, several gate concepts (i.e. gate-controlled, extended gate, back-gate) are also reported for different applications (Adzhri et al., 2016; Chen et al., 2011a, 2011b; Dattoli et al., 2012; Li et al., 2015).

2. Material and methods

2.1. Materials and reagents

Silicon-on-insulator (SOI) wafer was used as a substrate for the fabrication of silicon nanowires throughout this research. It was purchased from Soitec with 200 nm of buried oxide (BOX) and 50 nm of p-type Boron-doped silicon top layer (resistivity: 8.5–11.5 Ω cm). This fabrication process requires cleaning of the wafer using standard RCA 1 (mixing deionized (DI) water: 5, ammonium

hydroxide (27%): 1 and hydrogen peroxide (30%): 1), RCA 2 (mixing DI water: 6, hydrochloric acid (30%): 1 and hydrogen peroxide (30%): 1), hydrogen fluoride (HF) and buffered oxide etch (BOE) from Mallinckroot Baker. A positive resist (PR1-2000A), a negative resist (NR7-6000PY) and a resist developer (RD6), used for conventional lithography (pattern transfer) process, were purchased from Futurrex, Inc. Other required solutions including acetone, aluminum (Al) etch solution, ethanol and isopropyl alcohol (IPA) were purchased from Mallinckroot Baker. An SU-8 negative resist and an SU-8 developer solution used for microfluidic channel were purchased from MicroChem. To achieve nanometer-scale dimensions, the ma-N2400 series negative resist and ma-D 532 developer from Microresist Technology GmbH were used for the pattern transfer in direct-write electron beam lithography (EBL) process. The chemicals used for surface modification, 3-Aminopropyl triethoxysilane (APTES, 99%), glutaraldehyde and phosphate buffered saline (PBS; pH 7.4) were obtained from Sigma-Aldrich (M) Sdn Bhd. Moreover, all DNA oligomers related to dengue virus sequences were synthesized by AIT Biotech. A 27-mer amine-terminated probe (5'-NH₂-C₆-AAC AGC ATA TTG ACG CTG GGA GAG ACC-3') was used for DNA immobilization. To evaluate the specificity, sensitivity and control of DNA molecule detection, a 27-mer complementary target DNA (3'-TTG TCG TAT AAC TGC GAC CCT CTC TGG-5'), a 27 mer one-base mismatched DNA (3'-TTG TCG TAT AAC TGC GAC CCT TTC TGG-5') and a 27-mer non-complementary DNA (3'-CCT GTA CCG GGT CTA TGA TTG TGT CTT-5') were utilized. These DNA oligomers (100 μ M) were prepared in a TE buffer solution (10 mM Tris-(hydroxymethyl) aminomethane-HCl (Tris-HCl)+1 mM EDTA (pH 8.0)) (Sigma, USA) and kept frozen. All chemicals used throughout the experiment were of analytical reagent grade and used without further purification. All rinse processes were prepared with DI water (18 M Ω cm) from an ultrapure water system Millipore Billerica.

2.2. Development of silicon nanowire biosensors integrated with microfluidic channel

We previously reported the top-down nanofabrication approach of the silicon nanowires elsewhere (MN et al., 2016; Md Nor et al., 2013; Nuzaihan et al., 2013, 2015). Here, we summarize the main steps of the fabrication process (EBL process, inductively coupled plasma-reactive ion etching (ICP-RIE), size reduction process, conventional lithography and metal electrodes pad formation) and followed by the development of microfluidic channel. Briefly, a p-type SOI wafer was cleaned using RCA1, RCA2 and HF to remove organic and inorganic contaminations and native oxide layer on SOI surface. After the cleaning process, the SOI wafer was cut into small pieces (2 cm by 2 cm), and followed by EBL process. A 40–80 nm line structure was patterned using ma-N2400 series negative resist on the SOI substrate. ICP-RIE (a silicon dry etching process) was applied to form the silicon nanowires. To achieve the smallest possible width, the silicon nanowires were further trimmed via size reduction process by self-limiting thermal oxidation as previously reported (MN et al., 2016; Md Nor et al., 2013). The rest of the silicon nanowires were fabricated after the size reduction process. Subsequently, 150 nm of gold (Au) on a 10-nm titanium (Ti) electrodes were patterned on two ends of the fabricated silicon nanowires using lift-off process which involved conventional lithography for transfer pattern (electrodes structure) and metal deposition (Au/Ti) by a thermal evaporator. However, before placing the fabricated silicon nanowires into the evaporator, a short-buffered HF dip was performed to remove any native oxide covering the silicon nanowire pad. The HF soak time is crucial and thus needs to be optimized to avoid any removal of the buried oxide (BOX) and to maintain a layer isolating the electrodes from the substrate. Afterward, the open chamber

microfluidic channel was lithographically patterned and developed on the center of the fabricated silicon nanowire as previously reported (MN et al., 2016). Fabrication of the channel began with spin-coating the SU-8 resist at 300 rpm for 25 s on a cleaned silicon substrate surface and followed by a baking process at 90 °C for 75 min. The resulted thickness of the resist on top of the silicon substrate was approximately 100 μm. Then, the coated sample was exposed under ultraviolet (UV) light using a conventional lithography process for 240 s to transfer the channel geometry pattern onto the resist layer. Before developing process, the exposed sample was post baked at 90 °C for 15 min. The development of the sample was executed for various developing times using the SU-8 developer to determine whether the unexposed resist dissolved sufficiently. The dimensions of the open chamber microfluidic channel were 5 mm in length and 0.1 mm (100 μm) in width with 1.2-mm diameter inlet/outlet holes. The role of using microfluidic channel is to provide precision in delivery of various chemicals at small volume, thus serving indirectly as a passivation

layer to protect the electrodes pad from short-circuiting the sensing current. The development of silicon nanowire device was completed after the integration of microfluidic channel as schematically illustrated in Fig. 1(a).

2.3. Functionalization of silicon nanowire surfaces for molecular gate control

Functionalization of silicon nanowire surface with bio-recognition element (receptor molecules) is an important procedure for the development of biosensor, so that the device is capable and provides powerful set of tools for identifying a specific target molecule. The three steps involved in this functionalization are surface modification, DNA immobilization and DNA hybridization as schematically shown in Fig. 1(b). A chemical binding approach in the surface modification has been chosen in this research, to ensure that the targeted species are identified precisely, accurately and reliably. This approach is based on the binding of the probe

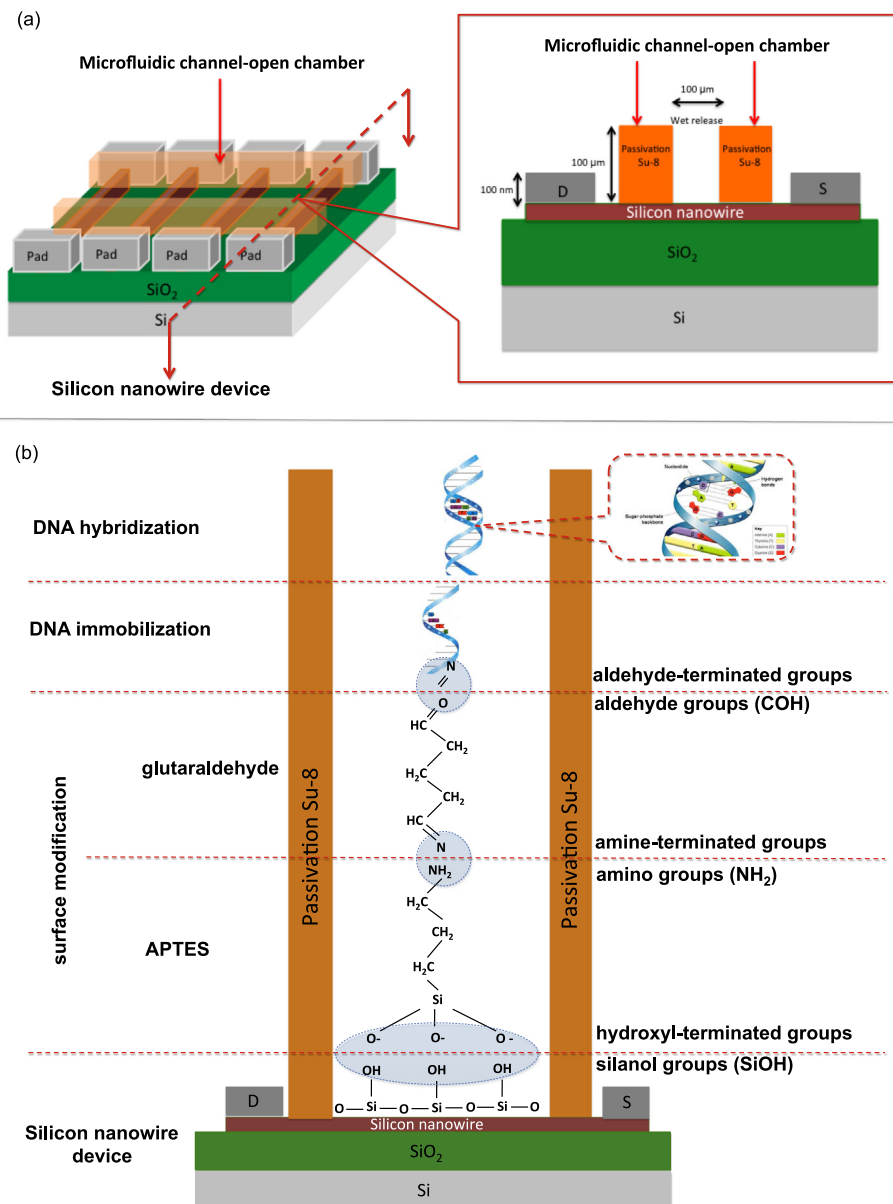


Fig. 1. Schematic illustration of (a) the silicon nanowire device integrated with microfluidic channel and (b) the surface functionalization, including surface modification by APTES and glutaraldehyde, DNA immobilization and DNA hybridization on the silicon nanowire surface.

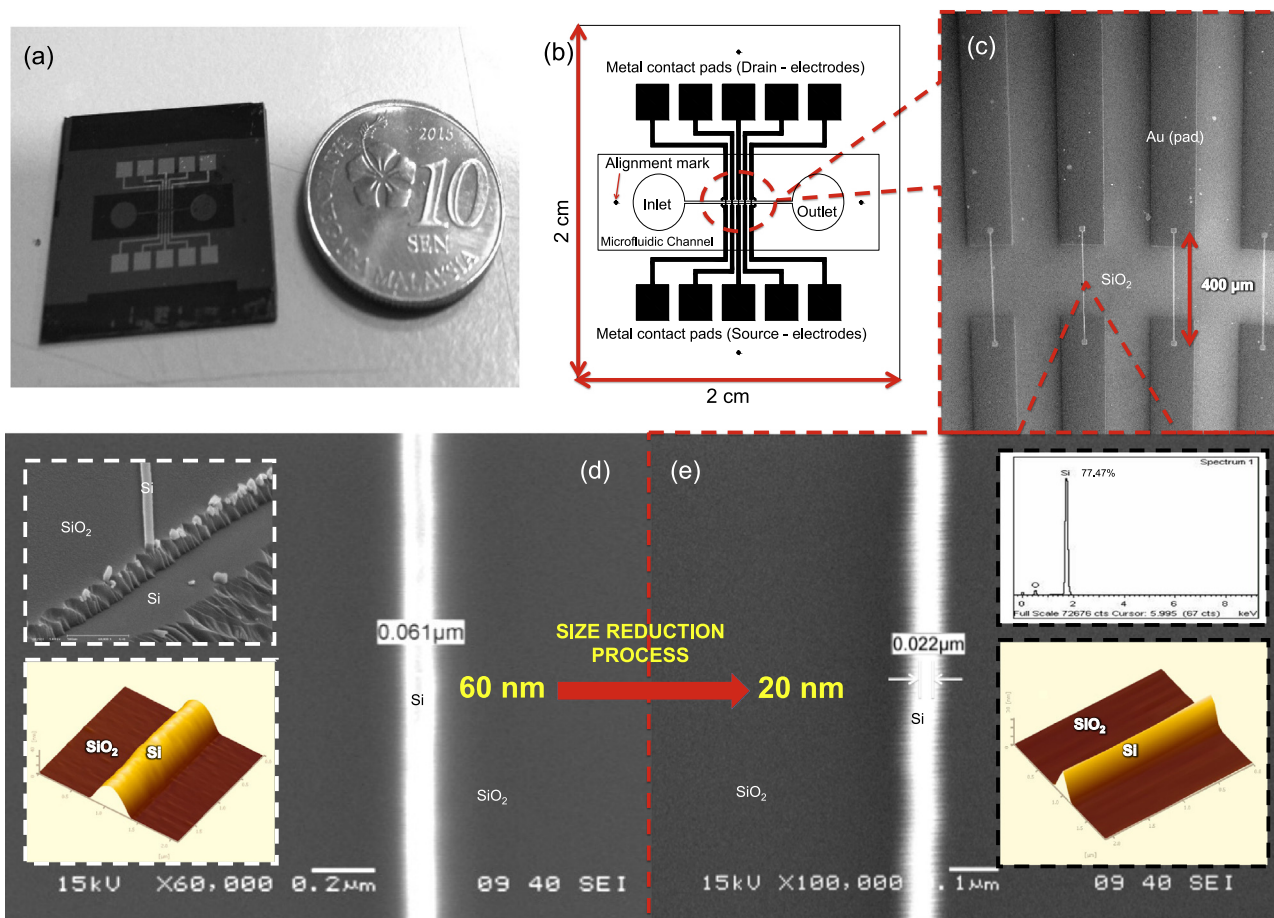


Fig. 2. Design of silicon nanowire biosensor: (a) The final structure of fabricated biosensor for DENV DNA detection. (b) The overall design for silicon nanowire biosensors with the microfluidic channel, drain and source electrode pads. (c) The SEM image of the silicon nanowire with different widths and 400- μm lengths. (d) The SEM image of silicon nanowire with 60-nm width and 50-nm height at 15 keV with 60,000 magnification. The insets are the cross-section and AFM image of the silicon nanowire before size reduction process. (e) The SEM image of 20-nm-wide and 30-nm-high silicon nanowires at 15 keV with 100,000 magnification. The insets are EDX spectrum and AFM image of the silicon nanowire after size reduction process.

molecule on the silicon nanowire surface by amine-based chemical bonds (Adam and Hashim, 2015). To activate the silicon nanowires in surface modification step, the native oxide layer (1–10 nm thick of SiO_2 , naturally oxidized and covalently bonded with hydroxyl groups (OH^-) to form silanol groups (SiOH) with excellent proton donors (H^+) and acceptors (SiO^-) present on the silicon nanowire surface was immersed in 2% 3-aminopropyltriethoxysilane (APTES (v/v)) in a mixture of 95% ethanol and 5% water for 2 h at room temperature to obtain surface-exposed- NH_2 (amine-terminated groups). In the meantime, the oxygen atom of the hydroxyl-terminated groups has performed a covalent bond with the silicon atom in the molecule of APTES. Then, the samples were cleaned using ethanol to remove any unreacted APTES and dried on a hot plate at 120 $^\circ\text{C}$ for 10 min. Subsequently, the APTES-functionalized silicon nanowire surface was immersed in 2.5% of glutaraldehyde (with PBS solution) and kept in the solution for 1 h at room temperature, followed by PBS cleaning and DI water rinse for 5 min to remove excess of glutaraldehyde. Glutaraldehyde was introduced as a linker to ensure a chemical bond with the amine-terminated groups and present aldehyde groups (COH) on the surface (Wenga et al., 2013). Aldehyde groups can subsequently be used for DNA immobilization step. For DNA immobilization, a 27-mer amine-terminated probe was linked to the aldehyde-terminated groups as shown in Fig. 1(b). A 10- μM DNA probe solution (diluted with PBS solution (pH 7.4)) was injected into the open microfluidic channel flowing through the silicon nanowire sensing area, followed by incubation process at room temperature for 4 h.

Next, any unbound probe was washed away with PBS solution. After immobilization step, a drop with 27-mer complementary DNA targets (10 fM to 10 μM concentrations) was injected into the sensing area to hybridize the immobilized DNA and kept hybridized sample by incubating at room temperature overnight. Then, the sample was washed again with PBS solution to remove the excess target DNA. To confirm the specificity of the biosensor, the sample was washed with hot DI water at 90 $^\circ\text{C}$ for 5 min to de-hybridize the complementary DNA pairs on the silicon nanowire surface, followed by sample hybridization with a 27-mer (same length) non-complementary DNA and one-base mismatched DNA. The sample has been stored at 4 $^\circ\text{C}$ when it is not in use.

2.4. Characterization of silicon nanowire biosensors

To ensure successful fabrication and functionalization of silicon nanowire biosensor, an electrical characterization was carried out to investigate the current-voltage (I-V), specificity and sensitivity of the silicon nanowire sensor using a KEITHLEY 6487 picoammeter/voltage source. The drain voltage was swept from 0 V to 1 V with the source grounded to test the fabricated silicon nanowires, the amine-terminated APTES, DNA immobilization and hybridization. Inspection and validation of the silicon nanowires during fabrication process were performed using high-power microscopy (HPM) (OLYMPUS-BX51) to make sure no contaminant was present, scanning electron microscopy (SEM) (JEOL JSM-6460LA) to determine the quality of the silicon nanowires

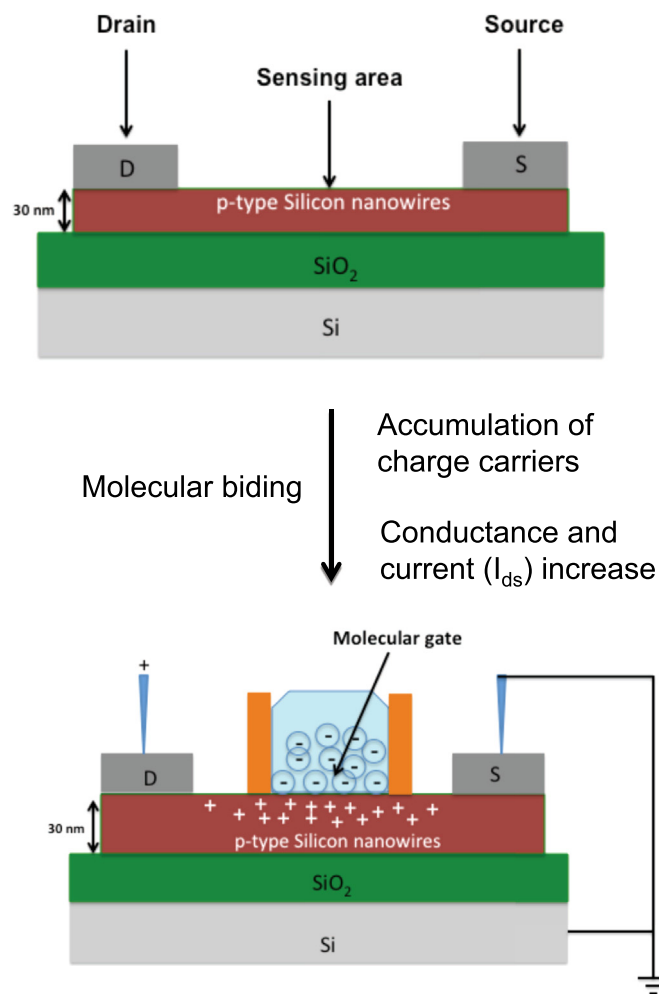


Fig. 3. The detection principle of silicon nanowire biosensors with novel molecular gate control.

(particularly the shape, diameter and uniformity) and atomic-force microscopy (AFM) (SPA400-SPI3800, Seiko) to study the 3D profile surface of the silicon nanowires. In addition, the thin-film layer uniformity and thickness were observed using a Filmetrics F20-UV spectrometer. Energy Dispersive X-ray Spectrometry (EDX) was used to do elemental analysis on silicon nanowire surface to examine the purity of the materials.

3. Results and discussion

3.1. Biosensor layout and detection principle

In this research, a p-type silicon nanowire biosensor (device) was fabricated using a top-down nanofabrication approach (involves EBL, ICP-RIE, size reduction process etc) and thus are fully compatible with CMOS technology. The completed device has a dimension of 20×20 mm (400 mm² in area) as shown in Fig. 2(a). Fig. 2(b) shows the device consists of three main structures, which are nanowire patterns, pads and microfluidic channel structure. The AutoCAD was utilized to design the microwire (1 μm), pads and microfluidic channel while the nanowire patterns were designed with 5 different widths (40, 50, 60, 70 and 80 nm) using RAITH ELPHY Quantum GDSII Editor. The 400-μm lengths were patterned to ensure that the nanowires were in contact with the electrode pads (act as transducer channels between two metal contact pads) (Fig. 2(c)) and thus to increase the probability of

reaction of the analytes to the nanowire surface during testing. The SEM image of the silicon nanowire (before size reduction process) is shown in Fig. 2(d), which indicates that the width of the silicon nanowire is approximately 60 nm. The cross-sectional SEM and AFM image shown in the Fig. 2(d) inset further revealed that this nanowire exhibits almost a rectangular cross section with approximately 60 nm in width and 50 nm in height. To achieve the smallest possible width of silicon nanowire with a good aspect ratio, the 60-nm silicon nanowire was dry oxidized and then a grown SiO₂ was etched away (i.e., size reduction process), which resulted in a final width of 20 nm (Fig. 2(e)) as previously reported (MN et al., 2016). The EDX spectrum of the fabricated silicon nanowire is presented in the inset of Fig. 2(e). The amount of silicon (Si) and oxygen (O) elements were achieved around 77.47% and 22.53% from the total percentage weight, respectively. There is a strong Si peak at 1.8 KeV together with the O peak in the spotted nanowire, indicating that was silicon nanowire was successfully fabricated, while the AFM (Fig. 2(e) inset) shows the morphology and profile of the silicon nanowire with approximately 20 nm in width and 30 nm in height.

In our research, a p-type silicon nanowire, which acts as the sensing component is connected between the source (S) and the drain (D) electrodes. To detect a specific target, the silicon nanowire surface is then functionalized with a bio-receptor, which is worked as a “molecular gate” by the binding of a target DNA. This detection principle has also been demonstrated by our research group (Adam and Hashim, 2015, 2016). A drain-source voltage, (V_{ds}) applied to the silicon nanowires will allow current, (I_{ds}) to flow from the drain to the source. The density of charge carriers in the nanowire is then modulated by the molecular gate, which in turn affects the current, resistance and conductance of the silicon nanowire. In our research of a p-type silicon nanowire, the application of negative charge by means of a bio-receptor leads to an accumulation of charge carriers in the sensing area, resulting in an increase in the measured current (I_{ds}) and conductance, thus decreasing the resistance. This detection principle is called molecular gate control as schematically depicted in Fig. 3.

3.2. Effect of silicon nanowire widths on the electrical characteristics

The quality of the silicon nanowires with various widths (20 nm (after reduction process), 40 nm, 60 nm, 80 nm and 1 μm) were further characterized electrically by applying a direct current (DC) voltage swept from 0 V to 1 V (small voltage range). The measurement setup of the fabricated silicon nanowire is shown in the inset of Fig. 4(a). All these measurements have been taken at room temperature (under ambient condition) to identify good and unsuitable devices (Kulkarni et al., 2012). Fig. 4(a) shows the excellent output of the electrical characteristics, I_{ds} versus V_{ds} (I-V), which indicates that the silicon nanowire exhibited an almost linear relation (ohmic behavior). At $V_{ds}=1$ V, the fabricated silicon nanowire with width of 20 nm, 40 nm, 60 nm, 80 nm and 1 μm has demonstrated I_{ds} of 115 pA, 146 pA, 201 pA, 327 pA and 2.6 nA, respectively. It was also observed that the increase of width raises the amount of I_{ds} gradually as shown in Supplementary Fig. S1. The raise of current was caused by the decrease in resistance of the silicon nanowire as shown in Fig. 4(b). The average resistance value of silicon nanowire with 20 nm, 40 nm, 60 nm and 80 nm width were 4.2 GΩ, 4.0 GΩ, 3.7 GΩ and 2.1 GΩ, respectively. It was found that, a bigger width of silicon nanowire has a lower resistance, which is in good agreement with electrical resistance theory. This is also consistent with the results of a similar experiment performed by Park et al. (2010) and Fatimah et al. (2013). According to the theory, a smaller cross-sectional area (silicon nanowire) would strongly contribute to increase resistance (R) value;.

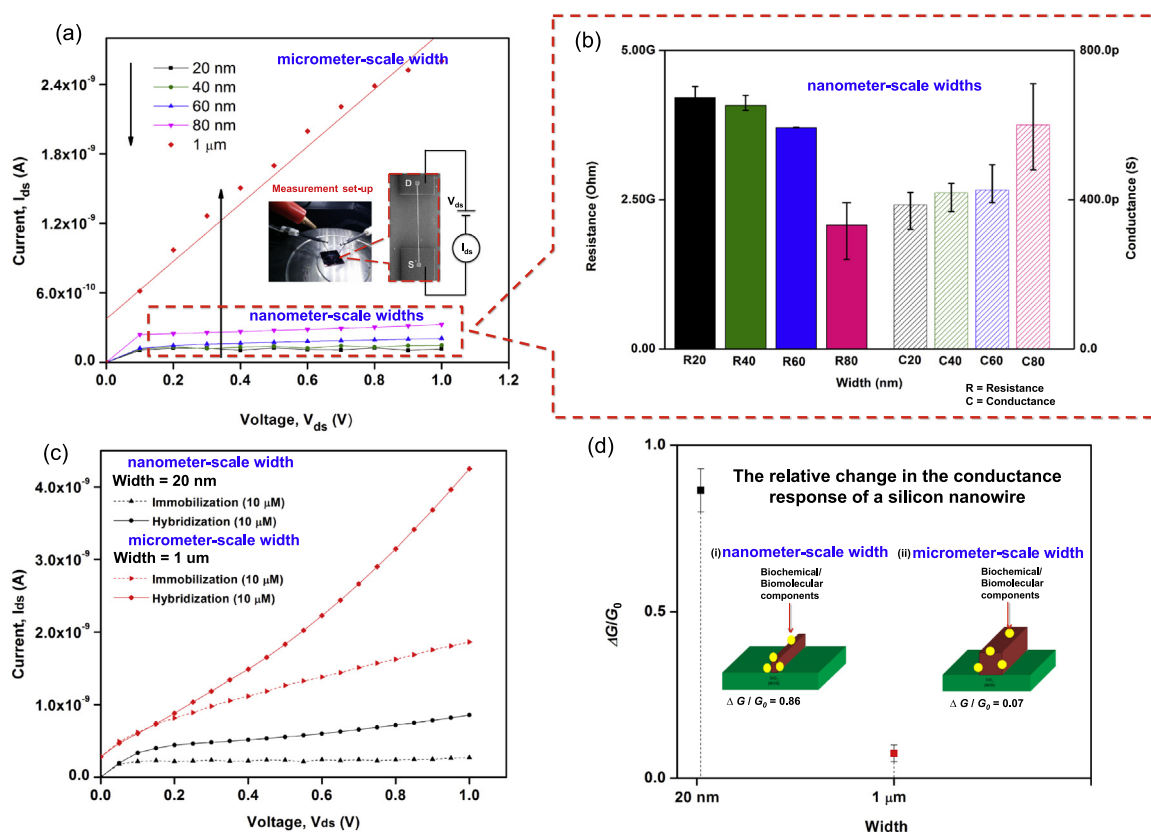


Fig. 4. Electrical properties of silicon nanowires: (a) I_{ds} - V_{ds} characteristic shows p-type ohmic behavior. (b) The resistance and conductance histograms of the silicon nanowire. (c) I_{ds} - V_{ds} characteristic shows the silicon nanowire width effect on the electrical characteristics to the surface functionalization. (d) The relative change in the conductance response of a wire for micrometer and nanometer-scale width.

$$R = \rho \ell / A \quad (1)$$

where ρ (rho) is the electrical resistivity of the material, ℓ is the length of the silicon nanowire and A is the cross-sectional area of the silicon nanowire (Chaudhry et al., 2007). It was also observed in histograms (Fig. 4(b)), that the average conductance value is inversely proportional to the average resistance value and clearly proportional to the width of silicon nanowire. Notably, these trends are in excellent agreement with previously reported (Delapierre et al., 2010).

To explore the silicon nanowire width effect on the electrical characteristics to the surface functionalization (DNA detection), two different silicon nanowire widths (1 μm (micrometer-scale width) and 20 nm (nanometer-scale width)) with the same length (400 μm) were compared. As shown in Fig. 4(c), there are significant differences in the measured I_{ds} values for each surface functionalization steps, exhibiting a well-defined molecular gate control of silicon nanowire field-effect sensors. Besides, it can be noted that the I-V characteristic for a bigger width is more linear than the smaller width of silicon nanowire (Park et al., 2010; Pennelli et al., 2011). For DNA hybridization (concentration, 10 μM), 1 μm width silicon nanowire showed higher measured I_{ds} =4.25 nA, compared to the I_{ds} =0.86 nA detected from the 20 nm width at V_{ds} =1 V. The same trend of measured I_{ds} value was observed for DNA immobilization (concentration, 10 μM), which is I_{ds} for 1 μm always higher than the I_{ds} for 20 nm. This clearly shows that, the I_{ds} values after DNA detection are highly dependent on the width of silicon nanowire. In addition, the current flow across the silicon nanowire is based on the depletion or accumulation of charge carriers when charged biomolecular components were attached on the surface of nanowire (Park et al., 2010), leading to a conductance change inside the silicon nanowire

(Chen et al., 2011a, 2011b). Furthermore, the conductance change is highly affected by the silicon nanowire widths with high surface-to-volume ratio (Chen et al., 2006; Hsiao et al., 2009; Li et al., 2014). For 1 μm width, the surface-to-volume ratio is relatively smaller compared to 20 nm due to a large interior area of the wire that might not be influenced by the electric field exerted from the charged biomolecular components (Fig. 4(d)ii inset), hence almost no significant alteration in conductance changes. The relative change in conductance for 1 μm width is 0.07, proving that a bigger width of silicon nanowire remains unaffected. In contrast, for 20 nm (smaller interior area), the surface-to-volume ratio was very large due to the influence of the external electric field, which could reach the whole cross-section of the nanowire (Fig. 4(d)i inset), resulting in large relative change in conductance, 0.86 (Agarwal et al., 2008). This could have been predicted, as scaling down width of silicon nanowire comes with an increase of the surface-to-volume ratio (Chen et al., 2011a, 2011b; Schmidt et al., 2010).

3.3. Analytical performance of silicon nanowire biosensors

As explained in Section 3.2 above, 20-nm p-type silicon nanowire has a large surface-to-volume ratio. Therefore, this transducer is believed to be highly sensitive to local charges in its environment. Nevertheless, suitable functionalization of silicon nanowire surfaces with correct biomolecular or biochemical components is required for a reaction to take place (Adam and Hashim, 2015). Further tests were conducted to evaluate the analytical performance metrics of 20-nm p-type silicon nanowire biosensor, which have been characterized in terms of its specificity, sensitivity, and LOD as shown in Fig. 5. In this research, the specificity of the silicon nanowire biosensors for the detection of DENV DNA was

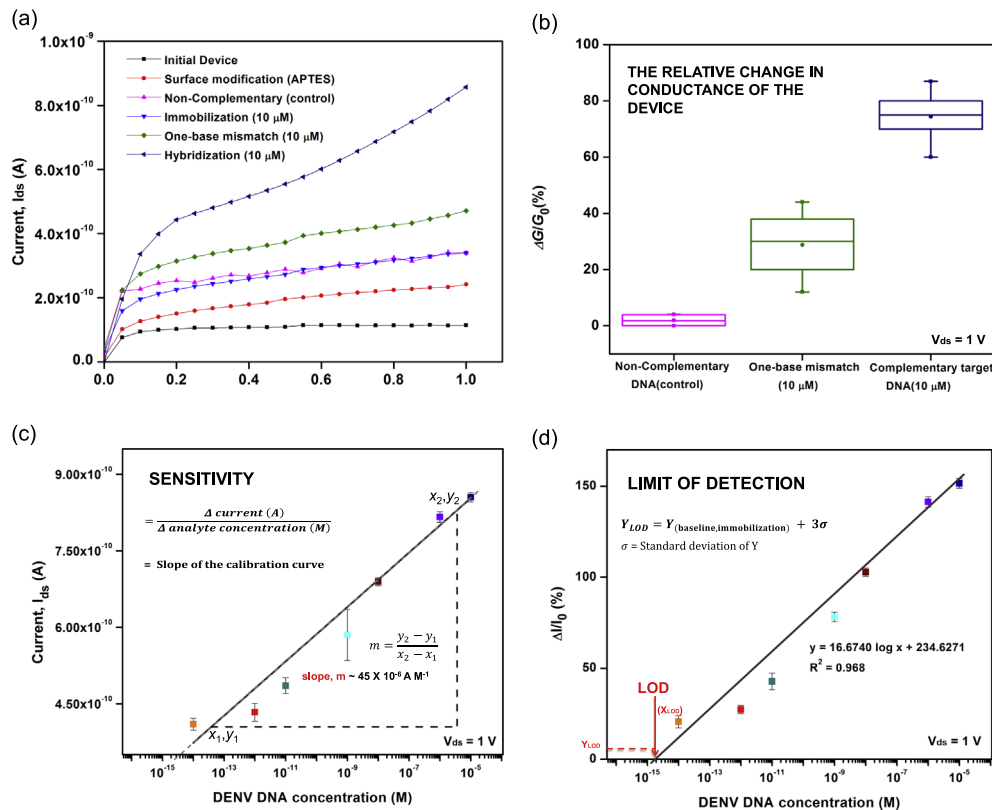


Fig. 5. Silicon nanowire biosensors: (a) I_{ds}-V_{ds} characteristic by different steps of surface functionalization. (b) Hybridization specificity demonstrated by the conductance to the complementary, one-base mismatched, non-complementary DNA sequences at V_{ds} = 1 V. (c) I_{ds} response curve of silicon nanowire biosensor with different concentrations of DENV DNA. (d) Calibration curve of the relative change in current, display limit of detection (LOD).

further verified by hybridizing a fully complementary target DNA, one-base mismatched target DNA and non-complementary target DNA (control group), both at same concentration of 10 μM, to the immobilized DNA probe. Fig. 5(a) clearly depicts the resulted I-V characteristics, which exhibited significant differences in the measured I_{ds} values for each of the DNA hybridization. It was observed that, upon hybridization with a fully complementary target DNA and one-base mismatched target DNA, an increase in current of 0.52 nA and 0.13 nA were recorded, respectively. However there was no change in the current that has been detected for non-complementary target DNA compared with the current of the immobilized DNA probe at V_{ds} = 1 V. The magnitude of this increase is dependent on the selectivity, which is typically achieved by attaching a specific recognition group to the surface of the silicon nanowire as explained in Section 2.3. In addition, the increment of the measured I_{ds} values is originated from the increased positive charges carrier current density on the p-type silicon nanowire encouraged by the negatively charged probe and target DNA (Ryu et al., 2010). Noteworthy, the contribution of any charge to the silicon nanowire induces changes in conductance and resistance accordingly (Zhang et al., 2009).

For further verification of the device specificity, the relative change in conductance of the device were plotted (Box Chart) as shown in Fig. 5(b). A negligible change in conductance (2%) was observed when a 10 μM of non-complementary target DNA was applied to the immobilized DNA probe. In contrast, an obvious significant change (74%) was observed when a fully complementary target DNA with the same concentration was used, while the conductance changes between one-base mismatched target DNA and the immobilized DNA probe resulted in a smaller increase in conductance (28%). The results indicated that only specific binding of target DNA to the immobilized DNA probe might induce the observed conductance changes. Simultaneously,

a similar trend was observed for the relative change in the resistance of the device as shown in Supplementary Fig. S2. The results disclose that the device offers a very good specificity with an excellent discrimination between fully complementary, one-base mismatched and non-complementary sequences, which is in good agreement with the previously reported results (Gao et al., 2007; Zhang et al., 2008, 2009, 2010).

To demonstrate the sensitivity and LOD of the silicon nanowire biosensor, the effect of different concentrations of fully complementary target DENV DNA, ranging from 10 fM to 10 μM were investigated. The I-V characteristics were plotted as shown in the inset of Fig. 5(c), which clearly showed the I_{ds} increased with increasing target DNA concentration. In other words, by adding and having more negative charge on the surface, the p-type silicon nanowire experiences accumulation of charge carriers (holes) around the perimeter of the silicon nanowire, resulting in an increase in the measured I_{ds} as explained in Section 3.1. The sensitivity of the device is the slope of the calibration curve (Fig. 5(c)) extracted from I-V characteristic (Supplementary Fig. S3). It was observed that I_{ds} increases linearly with increasing fully complementary DNA concentrations from 10 fM to 10 μM with the sensitivity of 45.0 μA M⁻¹ and thereafter saturated further. In addition to sensitivity, the LOD of the device should also be given a proper attention, which can be used to evaluate the ability of a device to detect the lowest concentration of an analyte in target DENV DNA. By calculating the relative change in the current of device to various concentrations of target DENV DNA, a calibration curve (the relative change in current were found to be well proportional to the natural logarithm of DENV DNA concentration) was plotted as shown in Fig. 5(d). The LOD of the device is approximately 2.0 fM. To the best of our knowledge, the sensitivity and LOD reported are among the best in detection of DENV DNA, compared to the previously reported in the literatures as shown in

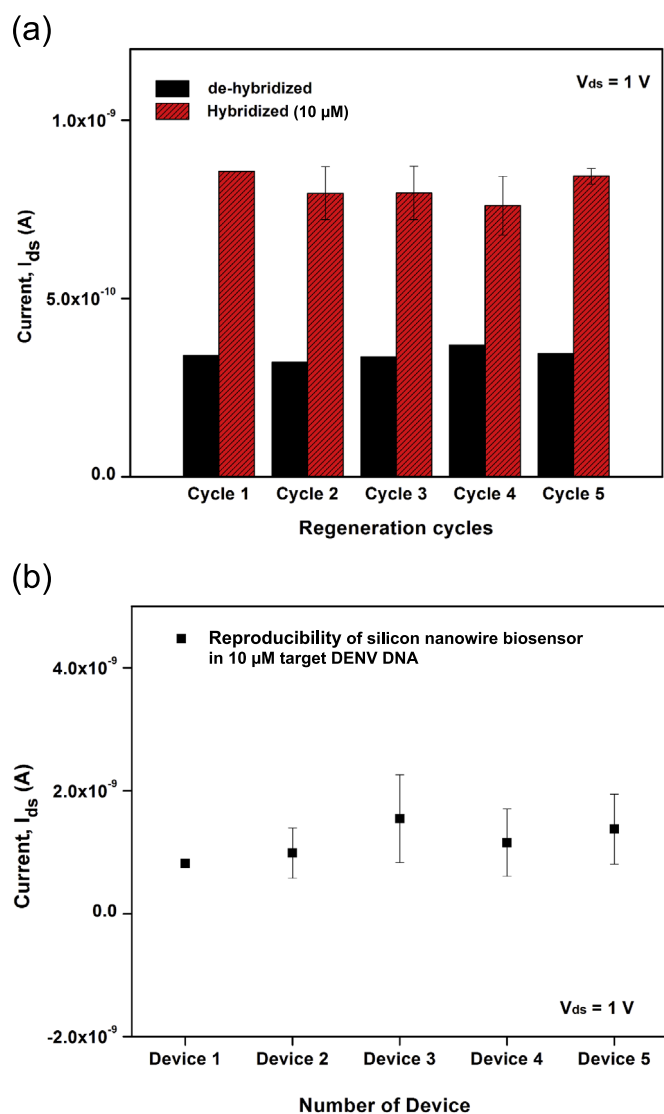


Fig. 6. (a) The repetitive cycles and (b) reproducibility of silicon nanowire biosensor in 10 μ M target DENV DNA.

Supplementary Table S1.

The device was further performed by monitoring the concentration-dependent conductance change upon hybridization to the complementary target DNA as shown in Supplementary Fig. S4. The relative change in conductance was extracted from the I-V characteristic as shown in Supplementary Fig. S3. An obvious 81.2% conductance change was obtained when 10 μ M concentration of complementary target DNA was hybridized to the immobilized DNA probe. However, the conductance change reduced to 73.8%, 66.0%, 36.8%, 23.8%, 12.2% and 6.8%, respectively when 1 μ M, 10 nM, 1 nM, 10 pM, 1 pM and 10 fM concentration of complementary target DNA were employed. From these obtained results, it can be concluded that the change in conductance after DNA hybridization is primarily dependent on the amount of the charge layer contributed by DNA. The more the target DNA was hybridized, the more negative charges added on the p-type silicon nanowires surface which lead to an accumulation of more positive charges carriers (holes), resulting in the increasing of the conductance values as observed. Furthermore, this observation was also in consistent with the literatures (Chen et al., 2011a, 2011b; Zhang et al., 2009). From this concentration-dependent conductance results, we have verified that our p-type silicon nanowire is feasible as a biosensor and it is obviously showed that this

biosensor provides a powerful electrical detection approach to detect target DENV DNA.

The capability of the sensor for repeated DENV DNA detection (repeatability performance) was investigated. The sensor (same device) was washed with hot DI water at 90 $^{\circ}$ C for 5 min to de-hybridize DNA pairs on the silicon nanowire surface (back to probe). The reusability of the sensor was tested by repetitive (five times) hybridization with same concentration of DENV DNA (10 μ M). The results of the sensor for repeatability performance were obtained as shown in Fig. 6(a). The I_{ds} values for five cycles (hybridization and de-hybridize) exhibited no significant change with negligible differences. A relative standard deviation (R.S.D) of hybridized regeneration cycles was found less than 5.0% for the same nanowire, suggesting a good repeatability of the proposed sensor. Further tests were conducted to evaluate the reproducibility of the sensor by comparing five different devices as shown in Fig. 6(b). As can be seen, the results have revealed a satisfactory reproducibility performance of the sensor with R.S.D was found slightly larger at 25.0% when compared to the repeatability performance. This might be due to a minor variation in the nanowire dimension and also the purity of the materials being used in the tests. Therefore, the silicon nanowire biosensors have a promising potential in monitoring of DENV DNA with stable and excellent repeatability and reproducibility performances.

4. Conclusion

We demonstrated a p-type silicon nanowire biosensor with a novel molecular gate control and the nanowire was scaled-down to 20 nm. The responsivity of this biosensor was thoroughly investigated by observing electrical detection in response to the concentrations of DENV DNA oligomer. It is shown that this electrical biosensor was able to detect as low as 2.0 fM concentration (LOD) with a greatly enhanced sensitivity of 45.0 μ A M $^{-1}$ with high specificity, repeatability and reproducibility. This research is useful in making novel electrical detection that can be commercialized for DNA detection. Thus, we expect this electrical biosensor to be beneficial for point-of-care diagnostic applications.

Acknowledgments

This research was supported by the Ministry of Higher Education Malaysia and Universiti Malaysia Perlis (UniMAP). The authors would like to thank all the team members of the Institute of Nano Electronic Engineering and School of Microelectronic Engineering (SoME), UniMAP for their technical advice and direct and indirect contributions.

Appendix A. Supporting information

Supplementary data associated with this article can be found in the online version at <http://dx.doi.org/10.1016/j.bios.2016.04.033>.

References

- Abdul Rashid, J.I., Abdullah, J., Yusof, N.A., Hajian, R., 2013. *J. Nanomater.* 2013, 1–16.
- Abdul Rashid, J.I., Yusof, N.A., Abdullah, J., Hashim, U., Hajian, R., 2016. *J. Mater. Sci.* 51, 1083–1097.
- Adam, T., Hashim, U., 2016. *Microsyst. Technol.* 22, 269–273.
- Adam, T., Hashim, U., 2015. *Biosens. Bioelectron.* 67, 656–661.
- Adzhri, R., Md Arshad, M.K., Gopinath, S.C.B., Ruslinda, A.R., Fathil, M.F.M., Ayub, R. M., Nor, M.N.M., Voon, C.H., 2016. *Anal. Chim. Acta* 917, 1–18.
- Agarwal, A., Buddharaju, K., Lao, I.K., Singh, N., Balasubramanian, N., Kwong, D.L.,

2008. *Sens. Actuators A Phys.* 145–146, 207–213.
- Baemner, A.J., Schlesinger, N.A., Slutzki, N.S., Romano, J., Lee, E.M., Montagna, R.A., 2002. *Anal. Chem.* 74, 1442–1448.
- Chaudhry, A., Ramamurthi, V., Fong, E., Islam, M.S., 2007. *Nano Lett.* 7, 1536–1541.
- Cheah, W.K., Ng, K.S., Marzilawati, A.-R., Lum, L.C.S., 2014. *Med. J. Malays.* 69, 59–67.
- Chen, C.-P., Ganguly, A., Lu, C.-Y., Chen, T.-Y., Kuo, C.-C., Chen, R.-S., Tu, W.-H., Fischer, W.B., Chen, K.-H., Chen, L.-C., 2011a. *Anal. Chem.* 83, 1938–1943.
- Chen, K.-I., Li, B.-R., Chen, Y.-T., 2011b. *Nano Today* 6, 131–154.
- Chen, S., Bomer, J.G., van der Wiel, W.G., Carlen, E.T., van den Berg, A., 2009a. *ACS Nano* 3, 3485–3492.
- Chen, S.-H., Chuang, Y.-C., Lu, Y.-C., Lin, H.-C., Yang, Y.-L., Lin, C.-S., 2009b. *Nanotechnology* 20, 215501.
- Chen, Y., Wang, X., Erramilli, S., Mohanty, P., Kalinowski, A., 2006. *Appl. Phys. Lett.* 89, 223512.
- Darwish, N.T., Alias, Y.B., Khor, S.M., 2015. *Trac. Trends Anal. Chem.* 67, 45–55.
- Dattoli, E.N., Davydov, A.V., Benkstein, K.D., 2012. *Nanoscale* 4, 1760.
- De Paula, S.O., Fonseca, B.A.L.D., 2004. *Braz. J. Infect. Dis.* 8, 390–398.
- Delapierre, G., Halté, C., Fournier, T., Baron, T., Gély, M., Buckley, J., De Salvo, B., Vinet, F., 2010. *Micro- and Nanotechnology. Sens. Syst. Appl. II*, 76792M.
- Dias, A.C.M.S., Gomes-Filho, S.L.R., Silva, M.M.S., Dutra, R.F., 2013. *Biosens. Bioelectron.* 44, 216–221.
- Fathil, M.F.M., Md Arshad, M.K., Gopinath, S.C.B., Hashim, U., Adzhri, R., Ayub, R.M., Ruslinda, A.R., Nuzaihan, M.N., Azman, M., Zaki, A.H., Tang, T.-H., M., 2015. *D. Biosens. Bioelectron.* 70, 209–220.
- Fatimah, S., Rahman, A., Yusof, N.A., Hashim, U., Nor, M.N., 2013. *Int. J. Electrochem. Sci.* 8, 10946–10960.
- Figueiredo, A., Vieira, N.C.S., dos Santos, J.F., Janegitz, B.C., Aoki, S.M., Junior, P.P., Lovato, R.L., Nogueira, M.L., Zucolotto, V., Guimarães, F.E.G., 2015. *Sci. Rep.* 5, 7865.
- Gao, Z., Agarwal, A., Trigg, A.D., Singh, N., Fang, C., Tung, C.-H., Fan, Y., Buddharaju, K. D., Kong, J., 2007. *Anal. Chem.* 79, 3291–3297.
- Gubler, D.J., 1998. *Clin. Microbiol. Rev.* 11, 480–496.
- Hahm, J., Lieber, C.M., 2004. *Nano Lett.* 4, 51–54.
- Hsiao, C.-Y., Lin, C.-H., Hung, C.-H., Su, C.-J., Lo, Y.-R., Lee, C.-C., Lin, H.-C., Ko, F.-H., Huang, T.-Y., Yang, Y.-S., 2009. *Biosens. Bioelectron.* 24, 1223–1229.
- Huang, M.J., Xie, H., Wan, Q., Zhang, L., Ning, Y., Zhang, G.J., 2013. *J. Nanosci. Nanotechnol.* 13, 3810–3817.
- Izuan, J., Rashid, A., Azah, N., Abdullah, J., Hashim, U., Hajian, R., 2014. *Mater. Sci. Eng. C* 45, 270–276.
- Kong, T., Su, R., Zhang, B., Zhang, Q., Cheng, G., 2012. *Biosens. Bioelectron.* 34, 267–272.
- Kulkarni, A., Xu, Y., Ahn, C., Amin, R., Park, S.H., Kim, T., Lee, M., 2012. *J. Biotechnol.* 160, 91–96.
- Lee, H.L., Rohani, A., Khadri, M.S., Nazni, W.A., Rozilawati, H., Nurulhusna, A.H., Nor Afzah, A.H., Roziyah, A., Rosilawati, R., Teh, C.H., 2015. *Int. Med. J. Malays.* 14, 11–16.
- Li, B.-R., Chen, C.-C., Kumar, U.R., Chen, Y.-T., 2014. *Analyst* 139, 1589.
- Li, J., Sun, M., Wei, X., Zhang, L., Zhang, Y., 2015. *Biosens. Bioelectron.* 74, 423–426.
- MN, M.N., Hashim, U., Md Arshad, M.K., Ruslinda, A.R., Rahman, S.F.A., Fathil, M.F.M., Ismail, M.H., 2016. *PLoS One* 11, e0152318.
- Md Nor, M.N., Hashim, U., Nazwa, T., Adam, T., 2013. *Adv. Mater. Res.* 832, 415–418.
- Monošík, R., Středanský, M., Šturdík, E., 2012. *Acta Chim. Slov.* 5, 109–120.
- Noor, M.O., Krull, U.J., 2014. *Anal. Chim. Acta* 825, 1–25.
- Nuzaihan, M., Hashim, U., Nazwa, T., Adam, T., 2013. *J. Appl. Sci. Res.* 9, 5580–5587.
- Nuzaihan, M.M.N., Hashim, U., Ruslinda, A.R., Arshad, M.K., Baharin, M.H.A., 2015. *Curr. Nanosci.* 11, 239–244.
- Oliveira, M.D.L., Nogueira, M.L., Correia, M.T.S., Coelho, L.C.B.B., Andrade, C.A.S., 2011. *Sens. Actuators B Chem.* 155, 789–795.
- Oliveira, N., Souza, E., Ferreira, D., Zanforlin, D., Bezerra, W., Borba, M., Arruda, M., Lopes, K., Nascimento, G., Martins, D., Cordeiro, M., Lima-Filho, J., 2015. *Sensors* 15, 15562–15577.
- Park, I., Li, Z., Pisano, A.P., Williams, R.S., 2010. *Nanotechnology* 21, 015501.
- Patolsky, F., Zheng, G., Hayden, O., Lakadamyali, M., Zhuang, X., Lieber, C.M., 2004. *Proc. Natl. Acad. Sci.* 101, 14017–14022.
- Patolsky, F., Zheng, G.F., Lieber, C.M., 2006. *Nat. Protoc.* 1, 1711–1724.
- Pennelli, G., Totaro, M., Bruschi, P., 2011. *Microelectron. Eng.* 88, 2368–2371.
- Rai, V., Hapuarachchi, H.C., Ng, L.C., Soh, S.H., Leo, Y.S., Toh, C.-S., 2012. *PLoS One* 7, e42346.
- Rashid, J.I.A., Yusuf, N.A., Abdullah, J., Hashim, U., Hajian, R., 2015. *IEEE Sens. J.* 15, 4420–4427.
- Rathakrishnan, A., Sekaran, S.D., 2013. *Expert Opin. Med. Diagn.* 7, 99–112.
- Ryu, S.-W., Kim, C.-H., Han, J.-W., Kim, C.-J., Jung, C., Park, H.G., Choi, Y.-K., 2010. *Biosens. Bioelectron.* 25, 2182–2185.
- Schmidt, V., Wittemann, J.V., Gösele, U., 2010. *Chem. Rev.* 110, 361–388.
- Shalev, G., Landman, G., Amit, I., Rosenwaks, Y., Levy, I., 2013. *NPG Asia Mater.* 5, e41.
- Silva, M.M.S., Dias, A.C.M.S., Silva, B.V.M., Gomes-Filho, S.L.R., Kubota, L.T., Goulart, M.O.F., Dutra, R.F., 2015. *J. Chem. Technol. Biotechnol.* 90, 194–200.
- Teles, F.R.R., Prazeres, D.M.F., Lima-Filho, J.L., 2005. *Rev. Med. Virol.* 15, 287–302.
- Teoh, B.-T., Sam, S.-S., Tan, K.-K., Danlami, M.B., Shu, M.-H., Johari, J., Hooi, P.-S., Brooks, D., Piepenburg, O., Nentwich, O., Wilder-Smith, A., Franco, L., Tenorio, A., AbuBakar, S., 2015. *J. Clin. Microbiol.* 53, 830–837.
- Tian, R., Regonda, S., Gao, J., Liu, Y., Hu, W., 2011. *Lab Chip* 11, 1952.
- Wenga, G., Jacques, E., Salaün, A.-C., Rogel, R., Pichon, L., Geneste, F., 2013. *Biosens. Bioelectron.* 40, 141–146.
- Wu, T.-Z., Su, C.-C., Chen, L.-K., Yang, H.-H., Tai, D.-F., Peng, K.-C., 2005. *Biosens. Bioelectron.* 21, 689–695.
- Yang, F., Zhang, G.-J., 2014. *Rev. Anal. Chem.* 33, 95–110.
- Za'bah, N.F., Kwa, K.S.K., Bowen, L., Mendis, B., O'Neill, A., 2012. *J. Appl. Phys.* 112, 024309.
- Zhang, G.-J., Chua, J.H., Chee, R.-E., Agarwal, A., Wong, S.M., 2009. *Biosens. Bioelectron.* 24, 2504–2508.
- Zhang, G.-J., Chua, J.H., Chee, R.-E., Agarwal, A., Wong, S.M., Buddharaju, K.D., Balasubramanian, N., 2008. *Biosens. Bioelectron.* 23, 1701–1707.
- Zhang, G.-J., Ning, Y., 2012. *Anal. Chim. Acta* 749, 1–15.
- Zhang, G.-J., Zhang, L., Huang, M.J., Luo, Z.H.H., Tay, G.K.I., Lim, E.-J.A., Kang, T.G., Chen, Y., 2010. *Sens. Actuators B Chem.* 146, 138–144.